frontiers in Built Environment

TYPE Original Research
PUBLISHED 12 March 2026
DOI 10.3389/fbuil.2026.1741805

OPEN ACCESS

EDITED BY
Paul Awoyera,
Prince Mohammad bin Fahd University,
Saudi Arabia

REVIEWED BY
Marialuigia Sangirardi,
University of Oxford, United Kingdom
Aref Maksoud,
University of Sharjah, United Arab Emirates

*CORRESPONDENCE
Paul A. Korswagen,
p.a.korswagen@tudelft.nl

RECEIVED 07 November 2025
REVISED 03 February 2026
ACCEPTED 04 February 2026
PUBLISHED 12 March 2026

CITATION
Prosperi A, Korswagen PA, Longo M and Rots JG (2026) Field observations of spatial surface temperature variations on masonry walls using infrared thermography.
Front. Built Environ. 12:1741805.
doi: 10.3389/fbuil.2026.1741805

Field observations of spatial surface temperature variations on masonry walls using infrared thermography

Alfonso Prosperi, Paul A. Korswagen*, Michele Longo and Jan G. Rots

Department of Materials, Mechanics, Management and Design (3MD), Faculty of Civil Engineering and Geosciences, Delft University of Technology, Delft, Netherlands

Temperature variations in masonry façades can induce expansion and contraction movements. When these movements are restrained, cracking and material degradation may occur, especially in older buildings lacking movement or expansion joints. Such temperature variations arise from factors as solar radiation, shading, material color, reflectivity, and environmental conditions. This study investigates the magnitude and spatial distribution of surface temperature variations (ΔT) on exterior masonry wall surfaces using outdoor infrared (IR) thermography. A better understanding of the magnitude and distribution of ΔT is essential for accurate damage assessment and for improving the attributability of observed damage to temperature effects rather than to other causes. Field data were collected in Delft, the Netherlands. Thermal images were captured with an IR camera to identify temperature differences across various points on exterior wall surfaces under direct solar radiation and varying shading conditions. The acquired imagery was analyzed using temperature histograms and profiles to quantify thermal gradients over the surface area of the façades. Results revealed significant spatial temperature variations, with measured ΔT values reaching up to 13 °C between the warmest and coolest zones on individual façades. Even where façades showed no pronounced surface gradients, temperature differences of up to 6 °C occurred between different, contiguous exterior walls of the same building. The study demonstrates that outdoor thermography, combined with targeted image processing, effectively identifies thermal gradients on masonry façades. These gradients reflect uneven thermal responses under real environmental conditions, which can accelerate moisture-related damage, cracking, and material fatigue. The findings emphasize the need to account for surface temperature heterogeneity in damage assessment of existing structures.

KEYWORDS
building diagnostics, infrared thermography, masonry façades, surface temperature gradients, thermal heterogeneity

1 Introduction

When materials undergo thermal changes, they tend to expand or contract (Thagunna, 2014). If these movements are constrained in buildings, stresses can develop within the walls, potentially leading to damage (see, for instance, Figure 1) (Rots, 1994; BRE, 1995; O'Connor and Droz, 1996; Van Zijl and Verhoef, 2001; Brick Industry Association, 2006; Dilrukshi and Dias, 2008; Gohnert, 2012; Almherigh, 2014; Gonçalves et al., 2015; Chitte and Sonawane,

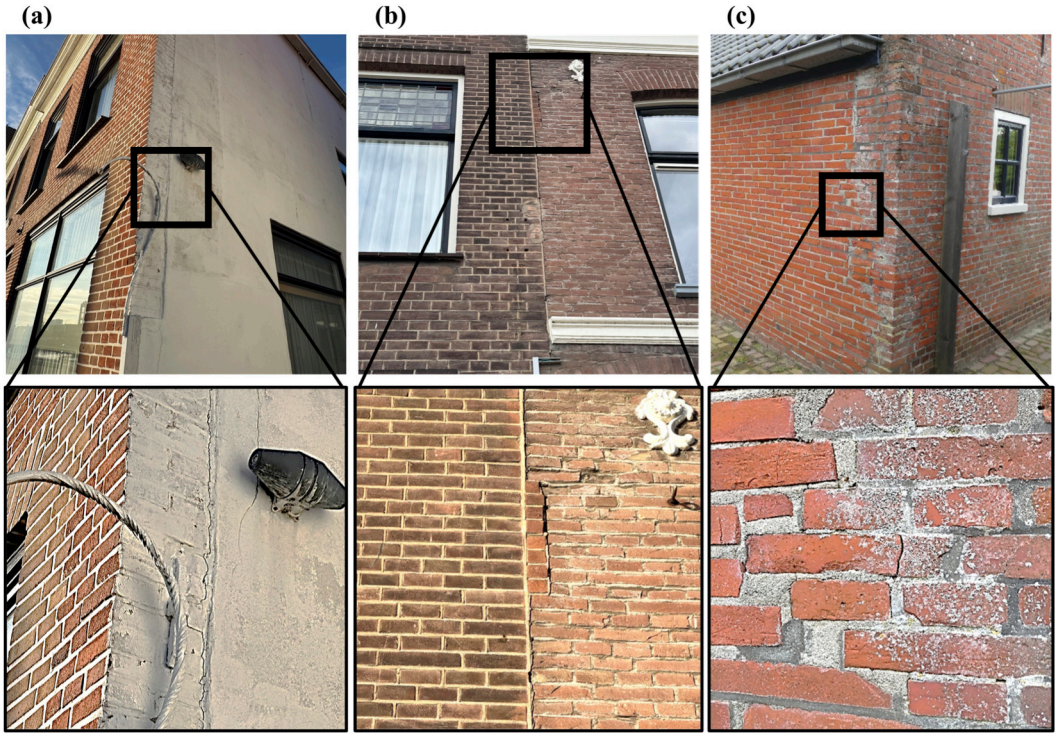

FIGURE 1
Examples of cracks that can be attributed to temperature effects: **(a,c)** cracks at the connection between façades and transversal walls; **(c)** damage that has been visibly repaired but reappeared over time; **(b)** vertical crack at the connection between two buildings: the crack mainly follows the vertical joint between the two structures, although some bricks also appear damaged. **(a,b)** are photographed by the Authors. **(c)** Courtesy of Instituut Mijnbouwschade Groningen (IMG).

2018; Miranda Dias et al., 2021; Latifi et al., 2023; Niedostatkiewicz and Majewski, 2024). While modern buildings are typically designed with movement and expansion joints to accommodate minor structural movements and prevent damage, either due to temperature variations or ground settlements (Farmer and Gerns, 2010; Mrozek et al., 2017; Kapusta and Szojda, 2021), older buildings often lack these features in their design. Therefore, the existing old unreinforced masonry structures, characterized by low tensile strength and a quasi-brittle behavior, can be particularly susceptible to both seasonal and daily movements due to temperature fluctuations (Farmer and Gerns, 2010; Prosperi et al., 2025b).

Masonry façades, which are directly exposed to different weather conditions, can experience significant temperature fluctuations, whereas sheltered components such as floors and foundations undergo much less thermal deformation (Holland, 2023). Temperature variations are not only observed through the cross-section of the walls (from the interior to the exterior of the building), but also over their surface. Temperature gradients over exterior walls' surfaces can result from the direct exposition to solar radiation (see, for instance, Figure 2), further influenced by shading effects, wall orientation, and heat transfer to the roof or foundation. Exposure to solar radiation and temperature fluctuations causes the external walls to deform differently from internal ones, inducing cracks in the connecting walls (Kleinfeld, 2004; Almherigh, 2014; Thagunna, 2014; Chauhan et al., 2020; Niedostatkiewicz and Majewski, 2024). In buildings with cavity walls that are filled with insulation, heat dissipation is reduced, causing the outer leaf of the wall to reach significantly higher temperatures than it would in a non-insulated cavity wall (Holland, 2023).

Due to temperature variations, cracking can occur, typically in the form of narrow vertical or horizontal cracks with relatively uniform width (Smith and Edgell, 2009; Dilrukshi and Dias, 2010; Yan et al., 2015; Miranda Dias et al., 2021; Holland, 2023). These cracks may open and close periodically, a phenomenon known as "breathing cracks" (Masciotta et al., 2016; Prosperi, 2025; Prosperi et al., 2025c), or deteriorate progressively over time (Ottoni and Blasi, 2015; Masciotta et al., 2016; Bauer et al., 2018; Chitte and Sonawane, 2018; Grandić et al., 2019; Miranda Dias et al., 2021; Sansara, 2023; Niedostatkiewicz and Majewski, 2024). After being repaired, cracks may reappear due to subsequent temperature variations (Sansara, 2023), as shown in Figure 1c. Even small cracks are undesirable in masonry buildings, not just for aesthetic reasons, but also because they can compromise the structure's watertightness, potentially causing further damage (Selvarajah and Johnston, 1995; Gaggero et al., 2024). Cycles of temperature variations can also affect protective layers like plaster coatings, increasing their susceptible to rain and snow penetration. Furthermore, ongoing climate change, with its rising temperatures and increasingly extreme weather events, can heighten the risk of damage, accelerating the aging process and material deterioration (Brimblecombe and Grossi, 2007; Roberts, 2008; Huijbregts et al., 2012; van Aarle et al., 2015; Lacasse et al., 2020; Athauda et al., 2023; Duan et al., 2025).

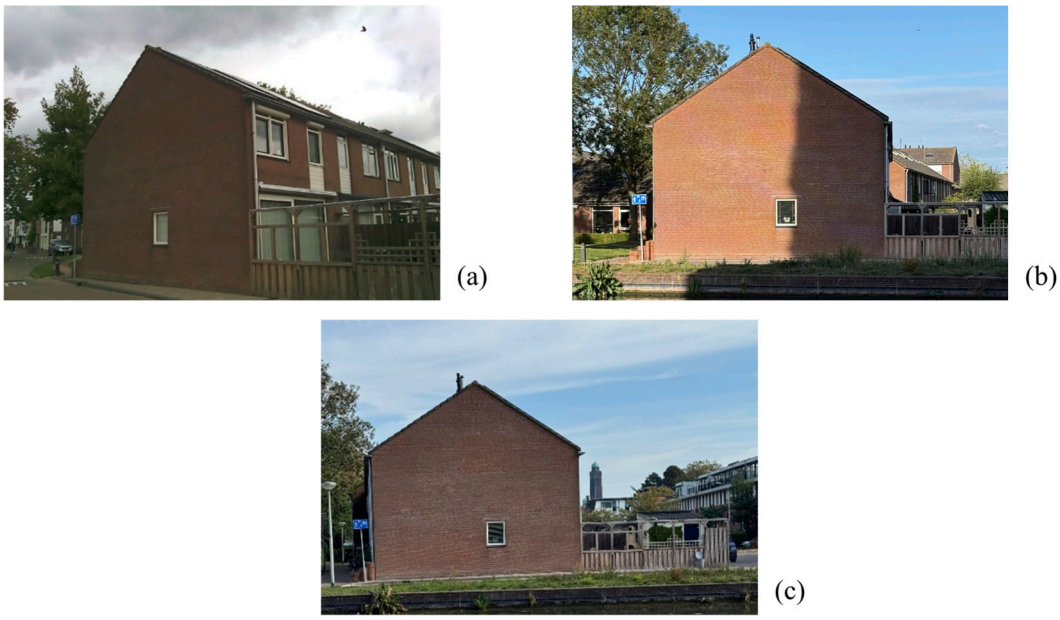

FIGURE 2
Photographs of an exterior wall of a residential building in Delft, taken on the 4th of September **(a)**, 8th of September **(b)**, and 1st of October **(c)** 2025. The comparison highlights variations in exposure to sunlight depending on the weather conditions and the sun's position.

Accurately identifying the causes and severity of damage is a crucial task not only to assess the condition of the buildings before implementing appropriate repair or strengthening measures but also for preventing further damage (De Vent, 2011; Latifi et al., 2023). Nevertheless, attributing damage becomes particularly challenging when cracking, especially if minor, may result from various causes, such as thermal effects, ground settlement, or vibrations (Holland, 2023). Although previous research has examined the effects of various sources of light damage, no study has quantitatively assessed the severity of damage resulting from the magnitude of temperature variations across façade surfaces. Gaining a deeper understanding of thermal variations over the façades of existing old buildings is essential for accurately evaluating structural behavior, guiding diagnostic surveys and maintenance strategies, and preventing further damage. This research seeks to address this critical gap in current knowledge.

In parallel, architectural research has explored computational and parametric design strategies aimed at generating environmentally adaptive building forms based on simulated thermal performance (e.g., Maksoud et al., 2023); however, such studies are design-oriented and differ fundamentally from empirical diagnostics of existing masonry façades, which form the focus of the present work.

Previous studies have primarily focused on how environmental variables affect building energy performance, with comparatively less attention given to their impact on the mechanical behavior of structures. For instance, research has frequently examined temperature differences between the interior and exterior of walls in the context of energy efficiency, heat flow, and moisture damage (Balaras and Argiriou, 2002; Yang et al., 2012; Marino et al., 2017; Chouidira et al., 2022; Barbero-Barrera et al., 2024). Additional studies focusing on structural behavior have explored how hygrothermal effects or restrained shrinkage of construction materials influence the structural response (Rots, 1994; Van Zijl et al., 2004; Beran, 2012; Ramirez et al., 2023; Pellegrini et al., 2024; Ramirez et al., 2024; Xia et al., 2025). In contrast, less attention has been given to temperature variations over the surface of exterior walls, such as differences between the top and bottom of a façade, or across its horizontal span. In (Yang et al., 2012), a predictive model was employed to assess the distribution of surface temperatures. The findings highlight solar radiation as the dominant factor influencing the thermal behavior of the façade. The model effectively captures shading and sunlit areas across different days and solar positions, demonstrating how temperature can vary significantly along external walls' surfaces. Similarly, other studies have examined how variations in solar radiation, driven by changes in daily hours, solar position, and shading, affect façade surface temperatures (Beran, 2012; Na et al., 2016; Chouidira et al., 2022; Barbero-Barrera et al., 2024). Temperature gradients over exterior wall surfaces have been assessed using IR outdoor thermographic techniques in (Na et al., 2016; Vollmer and Möllmann, 2018; Barbero-Barrera et al., 2024). In (Barbero-Barrera et al., 2024), the analysis revealed temperature differences of up to 7.4 °C between sunlit areas and those under solar protection during summer conditions, and up to 1.2 °C in winter across exterior wall surfaces. In (Na et al., 2016), the results indicate that both the magnitude and gradient of temperatures across the exterior walls of the surveyed structure varied throughout the day. In (Vollmer and Möllmann, 2018), a temperature difference of 17 K is observed in a house wall, comparing the location fully exposed to solar radiation and the one in shadow. The shadows lead to transient effects of solar load heating and cooling of the wall (Vollmer and Möllmann, 2018). Another noteworthy observation is that in (Na et al., 2016; Vollmer and Möllmann, 2018; Barbero-Barrera et al., 2024), outdoor IR

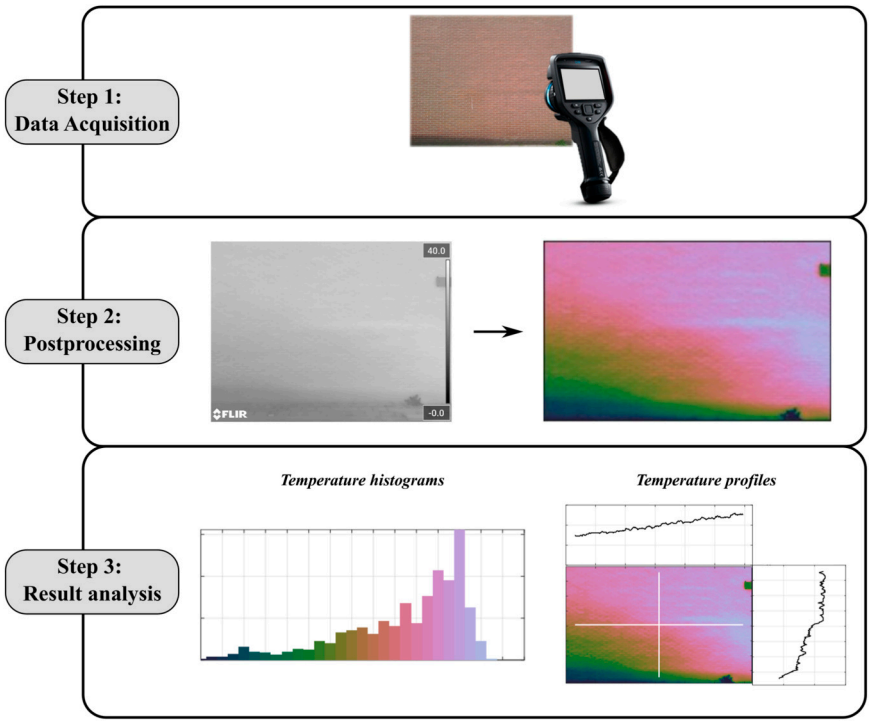

FIGURE 3
Flowchart of the adopted methodology.

thermography was employed to measure temperature variations over the areas of the walls' surfaces, an application that differs from their more traditional use in detecting heat loss or moisture infiltration (Vollmer and Möllmann, 2018; Richter and Fouad, 2021; Elizalde, 2025). This observation, along with the previously identified knowledge gaps, motivated the use of outdoor IR thermography in the present study to measure temperature variations across exterior wall surfaces.

This study contributes field-based quantitative evidence on the magnitude and spatial distribution of possible façade surface temperature differences (ΔT) on existing masonry buildings. This paper begins by introducing the methodology, available tools, datasets, and the study area in Section 2. The results of the analyses are shown in Section 3 and discussed in Section 4. Finally, Section 5 gathers the main findings.

2 Materials and methods

2.1 Methodology

The adopted methodology is composed of three steps, schematically illustrated in Figure 3, and detailed in the following:

- In Step 1, thermal imagery was acquired in the selected study area. Weather data are used in the calibration of the infrared camera used for the acquisitions. The data collection focuses on exterior masonry walls of existing old buildings.
- In Step 2, the collected data is processed using a MATLAB algorithm, developed for this application. The algorithm regulates the visibility and interpretability of subtle thermal variations across the masonry surfaces, enabling the systematic collection of information.
- In Step 3, the thermographic images are processed and analysed in detail. From the processed output, two types of information are collected:
  - Temperature histograms: provide insight into the magnitude of temperature differences over the analyzed façades surfaces.
  - Temperature profiles (or gradients): enable exploration of how temperature evolves along the height or length of the walls.

The analysis primarily focuses on evaluating temperature differences between specific points on the exterior walls, while absolute temperature values are of secondary importance.

2.2 Available buildings and weather data in the study area

The analyses entail observations of masonry buildings that were conducted in Delft, South Holland, Netherlands, on 4 September 2025 (Figure 4). In Delft, buildings span from pre-1700 constructions to modern developments (Kadaster, 2018; Peters et al., 2022). The city centre predominantly features low-rise houses, typically two to three stories high, built in continuous rows and finished with clay brick masonry veneers (Prosperi, 2025). The application is presented with reference to these buildings.

Insight into the weather conditions can be obtained from the data provided by the Royal Netherlands Meteorological Institute

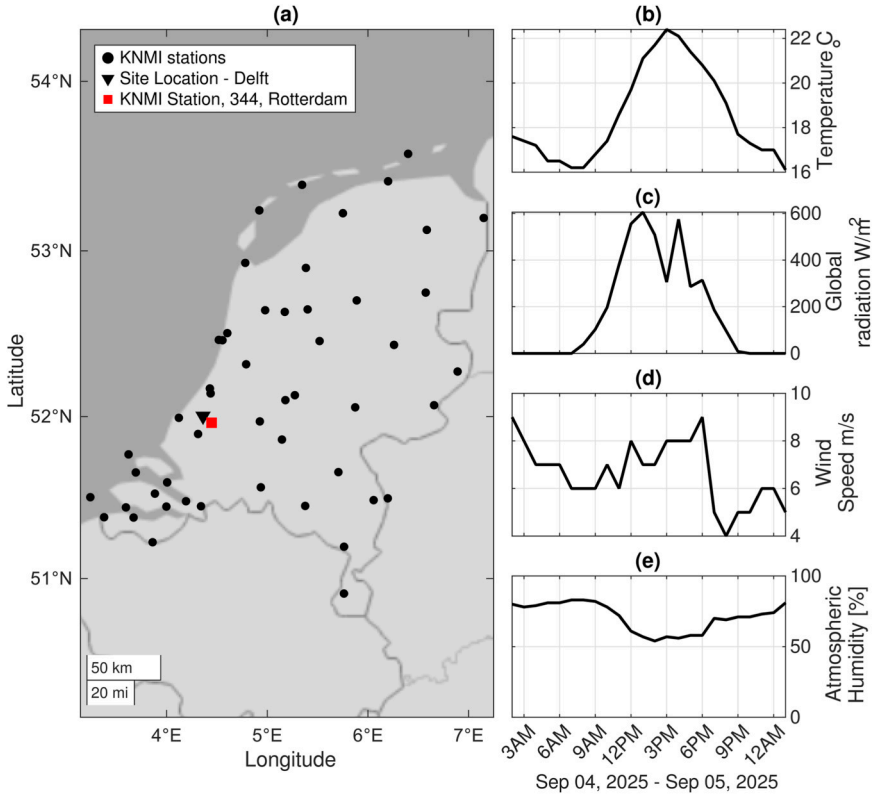

FIGURE 4
Weather conditions in the study area on 4 September 2025, based on freely accessible data from KNMI (www.knmi.nl). The infrared thermographic survey was conducted between 1:00 p.m. and 2:30 p.m. **(a)** Map of the Netherlands and KNMI weather stations. **(b–e)** Hourly temperature, solar radiation, wind, and relative humidity, respectively, for the 4th of September 2025.

(KNMI), which is freely accessible at www.knmi.nl. The closest meteorological station is located in Rotterdam (Station 344), as shown in Figure 4a. The nearest KNMI station (Rotterdam, Station 344) was used following standard practice; these data serve only for camera calibration, while the analysis focuses on relative temperature differences (ΔT), which are insensitive to small spatial variations in meteorological inputs.

The data collection excursion ("Step 1" in Figure 3) took place from approximately 1:00 p.m. to 2:30 p.m. local time. The field excursion was carried out during the hottest time of the day (approximately 22 °C–23 °C) and under the highest solar radiation (as shown in Figures 4b,c). Wind speed during the survey was approximately 7–8 m/s, slightly above the regional average of 5–6 m/s (Yemer, 2010). The atmospheric humidity was estimated to be around 50% (Figure 4e). These insights are used as input for the infrared device in the following analysis.

2.3 Outdoor infrared thermography

Thermography is a non-destructive, non-contact, and non-invasive technique that measures the intensity of infrared radiation emitted by a surface or object to determine its temperature (Vollmer and Möllmann, 2018; Richter and Fouad, 2021; Kim et al., 2023; Elizalde, 2025). IR thermography is often employed for monitoring and analyzing the thermal behavior of structures (Plesu et al., 2012; Kim et al., 2023; Elizalde, 2025).

TABLE 1 An overview of the parameters used with the thermal camera FLIR E96 during the field excursion.

Object distance	3.0 m
Atmospheric temperature	20 °C
Relative humidity	50%
Reflected temperature	22 °C
Emissivity	0.95

In this study, *in situ* IR imagery was acquired ("Step 1" in Figure 3) using the FLIR E96 thermal camera, which features a resolution of 640 × 480 pixels with 1.2 megapixels, using a 42°, 10 mm lens. The device was configured to operate within a temperature range of −20 °C to +120 °C, with an internal tolerance deviation of ±2% (Flir Systems, 2024).

The IR camera calculates and displays temperature as a function of the emitted infrared radiation, which depends on the emissivity and the environmental conditions (Barreira and de Freitas, 2007). The emissivity describes a material's capacity to emit infrared radiation (Richter and Fouad, 2021; Elizalde, 2025). Emissivity is expressed as a value between 0 and 1.0, where 0 represents a body that emits no infrared radiation and reflects all surrounding

radiation, and 1.0 represents a perfect emitter radiating the maximum infrared energy for its temperature. In civil engineering thermography, the emissivity of brick masonry is typically estimated between 0.90 and 0.95. For this application, the emissivity is set to 0.95 (Table 1). For objects with high emissivity, small changes in the selected emissivity value result in only minimal differences in the measured surface temperature (Usamentiaga et al., 2014).

During the acquisition, the adopted thermal camera also compensates for the effect of different radiation sources based on the parameters listed in Table 1 (Flir Systems, 2019). In detail, the object distance is used to compensate for the radiation absorbed by the atmosphere between the target surface and the camera, as well as for the thermal radiation emitted by the atmosphere itself. The selected object distance is set at 3 m, although the influence of this parameter is expected to be negligible, as it is typically only significant for distances greater than 20 m (Chew, 1998). The relative humidity represents the moisture content of the surrounding air, and the camera manufacturer recommends using a default value of 50% when specific data are not available (Flir Systems, 2019), consistent with the one measured during the field excursion (Figure 4e). The atmospheric temperature, representing the air between the camera and the target, was determined based on meteorological data collected during the field excursion (Figure 4). The apparent reflected temperature compensates for the portion of environmental radiation reflected by the object, although this effect is generally less relevant for surfaces with high emissivity (Usamentiaga et al., 2014). To reduce the number of variables and focus on the surface temperature, all image acquisitions were performed using consistent settings. In general, emissivity is expected to be the most influential parameter for this application. Object distance, atmospheric temperature, and relative humidity become significant mainly for targets located far from the camera, while reflected temperature is more relevant for objects with low emissivity (Flir Systems, 2017). As previously mentioned, this study primarily focuses on evaluating temperature differences between specific points on the exterior walls. Therefore, absolute temperature values, which may be influenced by the chosen imaging parameters, are considered of secondary importance. The underlying hypothesis is that the selected camera parameters affect the absolute temperature values to a greater extent than the temperature differences (ΔT) between points. This hypothesis will be discussed in the following, as the camera parameters can be adjusted retrospectively through the camera interface. As the targets are static façade surfaces and acquisition times are short, handheld operation does not affect spatial temperature distributions or ΔT measurements.

While thermographic images are typically displayed using pseudocolor scales, where cooler temperatures are shown in shades of blue and warmer temperatures in shades of red (Playà-Montmany and Tattersall, 2021; Elizalde, 2025), in this study, a "White hot" color palette was applied to all images, with a fixed temperature scale ranging from 0 °C to 40 °C. The selected color palette allowed the thermal images to be treated as grayscale images, where each pixel corresponds to a single numerical brightness value ranging from 0 (black) to 255 (white). In contrast, using a multicolor palette would have required three values per pixel (red, green, and blue components), complicating post-processing and increasing computational load without necessarily improving the precision of temperature analysis.

The camera settings were adjusted to minimize overlay information on the thermal images, thereby maximizing the investigated area in the pictures. The camera was manually operated by a technician during the data collection process, without a tripod, to allow for quick movement between locations.

2.4 Postprocessing of the thermal images

Thermal images were post-processed using a MATLAB-based script to enable more detailed analysis beyond the camera's raw output ("Step 2" in Figure 3). The program automatically identified the maximum and minimum surface temperatures in each image and thus allowed a flexible adjustment of the color palette and temperature range displayed. These features enhanced the visibility and interpretability of subtle thermal variations over the masonry surfaces but did not alter nor process the data stored in the image, where temperature values are simply stored as an RGB-triplet. Moreover, the program allowed the selection of specific areas of the images, facilitating focused analysis of localized wall sections and enabling precise quantification of temperature variations over specified lines.

From the processed images, temperature histograms and temperature profiles along the height and surfaces of the investigated walls were obtained in Step 3 of the adopted methodology (Figure 3).

3 Results

3.1 Examples of thermal images

Figure 5 provides two examples of buildings for which thermal images were acquired during the field excursions. The figure demonstrates how the original thermal images obtained using the camera protocol described in Section 2, with a temperature scale ranging from 0 °C to 40 °C, are post-processed with a custom temperature range from 20 °C to 35 °C, selected to regulate the visibility of temperature measurements, and a custom color palette. Similar comparisons between the original raw thermal images and the post-processed ones were carried out preliminarily to test the reliability of the algorithm and the overall procedure.

From the examples in Figure 5, well-known effects that can distort temperature readings are evident. For instance, metallic surfaces or windows may produce inaccurate readings due to their significantly different emissivity characteristics. In such cases, the thermal camera may capture reflected infrared radiation from the environment, such as the sky, rather than the true temperature of the surface (Vollmer and Möllmann, 2018). Areas of different materials that are dark in color and have a rough texture reflect less light, causing their temperature to increase more quickly (Chitte and Sonawane, 2018). However, this study does not investigate the temperature gradients on these materials and thus the difficulty in capturing their surface temperature with infrared thermography is not relevant. The focus lays on the masonry bits of brick façades whose temperature can be reliably observed.

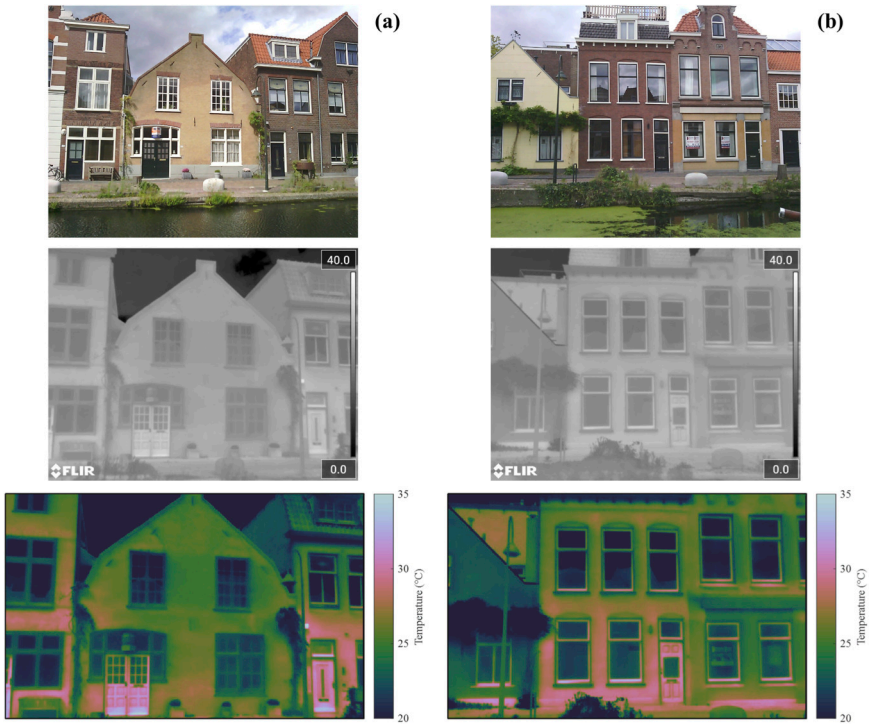

FIGURE 5
Two examples **(a,b)** of thermal images of two buildings acquired in Delft on 4 September 2025. The figure illustrates the difference between the photographs (top), the original thermal images obtained using the camera protocol described in Section 2 (middle), and the post-processed results produced by the MATLAB algorithm (bottom), which allow flexible adjustment of the color palette and temperature range.

Both buildings appear to have areas at the bottom of the façades hotter than the ones at the top. It is possible to observe that both buildings are located in front of water canals (Figures 5a,b). Therefore, the infrared radiation reflected from the body of water or from the street may have influenced the readings. For this reason, these images were excluded from the subsequent analysis, and different buildings were selected instead.

Moreover, Dutch masonry buildings are characterized by the presence of large daylight openings in their facades (Messali et al., 2018; Arslan et al., 2021; Prosperi, 2025; Prosperi et al., 2025a). This aspect represents a limitation for the analysis, as the available masonry area for evaluating temperature differences may be restricted in buildings like the one shown in Figure 5. For this reason, in the following histograms of temperature differences are shown for a case without large openings, whereas temperature profiles are presented for all the other cases.

3.2 Temperature histograms and temperature profiles

Figure 6 shows a building with a tall (approximately 8 m in height) transversal wall with only one small opening. Thermal images were acquired from three distinct viewpoints (Figure 6a), with a time interval of approximately 30–60 s between successive acquisitions. During the acquisitions, the façade was initially exposed to direct sunlight (Observation Point 1, Figure 6b), then partially shaded, likely due to cloud cover (Observation Point 2, Figure 6c), and subsequently illuminated again by direct sunlight (Observation Point 3, Figure 6d). The corresponding thermal images are shown in Figures 7–9. In all three figures, the considered temperature range has been limited to values between 20 °C and 35 °C, whereas temperature histograms (Figures 7c, 8c, 9c) reveal the temperature ranges only over the surface of the considered wall. All three histograms resemble lognormal distributions of the temperature values. The lognormal shape of the histograms indicates that most of the wall's surface exhibits higher temperatures, while a smaller portion of the wall shows lower temperatures, as reflected by the left-hand tail. Indeed, the approximately lognormal temperature distributions indicate localized thermal extremes rather than uniform gradients, highlighting the heterogeneous thermal response of masonry façades.

Figure 7c shows that from the bottom left to the top right of the wall, a temperature difference (ΔT) of approximately 13 °C is observed, ranging from around 21 °C to 34 °C. Even excluding the influence shaded area at the bottom of the façade close to the ground, thus the values of the lower tail of the histogram, a temperature gradient of about 9 °C is detected, with values ranging from approximately 25 °C to 34 °C. Another important observation is the abrupt temperature variation at the corner of the two orthogonal façades (Figure 7a), a location often prone to cracking (see Figure 1).

The histogram shown in Figure 8c shows a temperature range ΔT of approximately 7 °C, spanning from around 24 °C to 31 °C. From this viewpoint, the shaded area at the bottom of the façade is not included in the image; consequently, lower temperature values

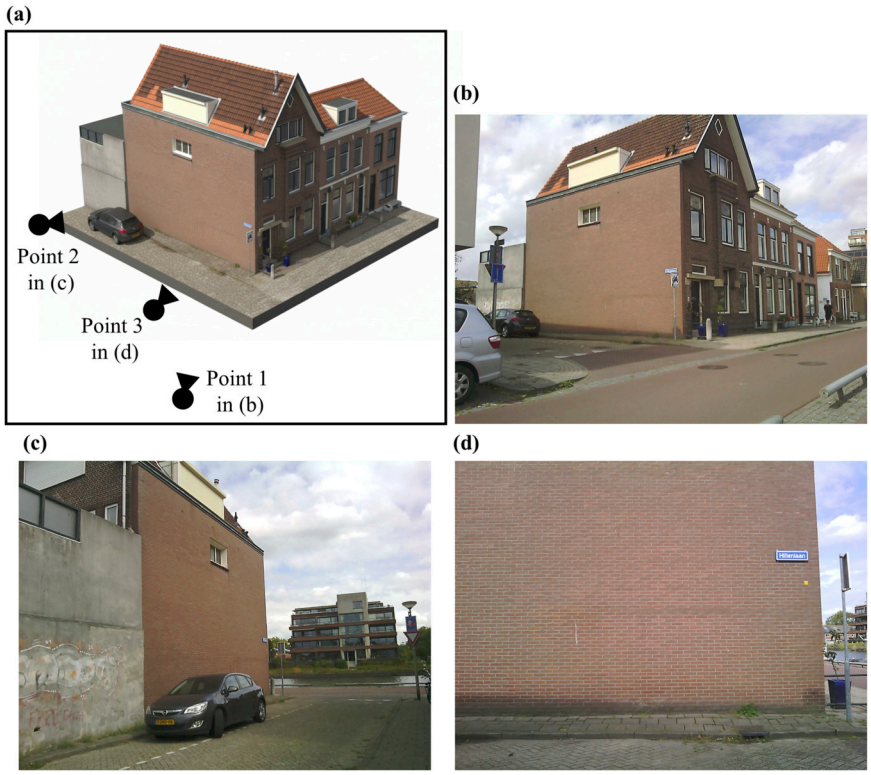

FIGURE 6
Building in Hillenlaan (Delft), including three points of observation. The corresponding thermal images are analyzed in Figures 7–9. Timestamps (local time): **(a)** 1:26:28 p.m., **(b)** 1:27:26 p.m., and **(c)** 1:28:18 p.m. **(a)** Isometric view of the selecting building (illustration). **(b)** Observation point 1. **(c)** Observation point 2. **(d)** Observation point 3.

are absent from the histogram. The slightly lower maximum temperatures (~32 °C) compared to the previous viewpoint (~34 °C in Figure 7c) may be attributed to reduced direct solar exposure and the different observation point. In Figure 7c, the higher temperature values could be partially influenced by solar radiation reflected from the wall surface (Vollmer and Möllmann, 2018). Additionally, although only a few seconds elapsed between the two acquisitions, a slight cooling of the wall cannot be excluded. As reported by (Vollmer and Möllmann, 2018), temperature differences of a few degrees can occur within just a few minutes after solar irradiation ceases, depending on material properties and environmental conditions.

The results for the third viewpoint are shown in Figure 9, again under direct sunlight. The image, acquired from a closer distance to the wall, covers approximately half of its length and only a portion of its height (Figure 6d). Once again, a ΔT of about 9 °C is observed, from approximately 25 °C to 34 °C.

Despite the differences in absolute temperature values between the three images, they exhibit a consistent spatial distribution and similar magnitudes of temperature differences (ΔT), which are central to this analysis. These observations indicate that, although absolute temperature measurements are well-known to be influenced by external factors (Vollmer and Möllmann, 2018; Richter and Fouad, 2021; Kim et al., 2023; Elizalde, 2025) (direct solar radiation, in this case) and thus not fully reliable, the methodology employed in this study, and similarly in prior research (Barbero-Barrera et al., 2024), remains valid for analyzing temperature differences and spatial patterns.

Vertical (along the wall height) and horizontal (along the wall length) temperature profiles are shown for two different cases in Figures 10, 11. In Figure 10, a temperature difference along the horizontal profile of about 4 °C can be observed between areas in shadow and under direct sunlight. Moreover, a difference of about 5 °C–6 °C can be observed between the left portion of the front façade and the transversal wall.

In contrast, in Figure 11, the temperature profiles do not reveal any particular temperature difference along the lines. Nevertheless, also in this case, a temperature difference of approximately 5 °C–6 °C can be observed between the two walls. These differences may stem not only from tree shading or proximity to other structures, but also from the sun's path around the building.

4 Discussion

4.1 Comparison with prior studies

The literature survey revealed a notable gap in studies specifically addressing temperature variations over exterior wall surfaces. Existing research has predominantly focused on the influence of solar radiation and sun position on building energy performance, with limited attention to the structural implications of these thermal effects. Although it is well established in engineering

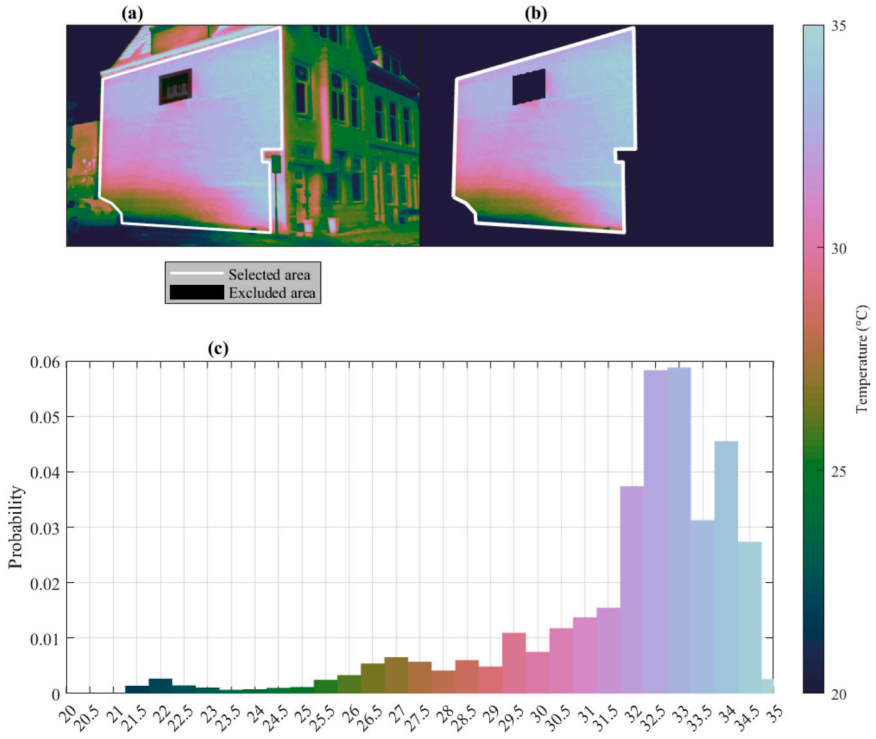

FIGURE 7
Analyses of the thermal image from observation point 1 in Figure 6. Temperature values progressively increase from the lower-left corner of the wall toward its right side. **(a)** Processed thermal image. **(b)** Selected area. **(c)** Temperature histogram (°C) of the selected area.

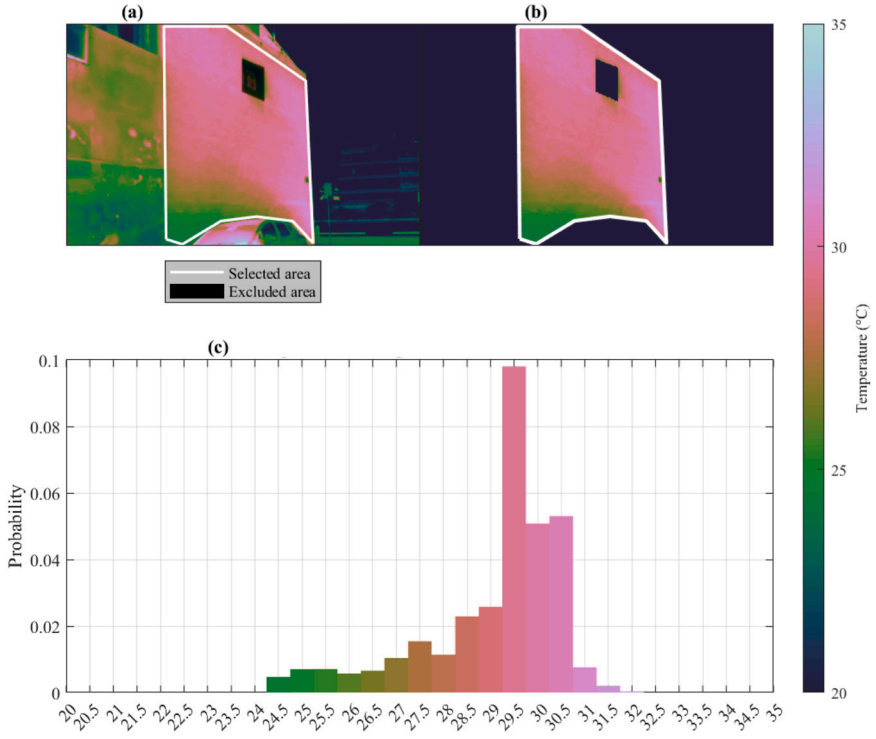

FIGURE 8
Analyses of the thermal image from observation point 2 in Figure 6. Temperature values exhibit a similar pattern to those shown in Figure 7. **(a)** Processed thermal image. **(b)** Selected area. **(c)** Temperature histogram (°C) of the selected area.

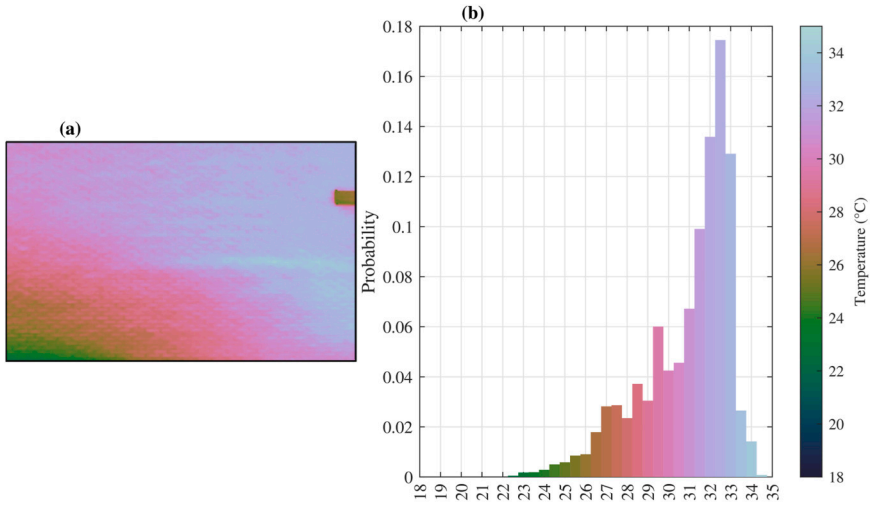

FIGURE 9
Analyses of the thermal image from observation point 3 in Figure 6. Temperature values exhibit a similar pattern to those shown in Figures 7, 8. **(a)** Processed thermal image. **(b)** Temperature histogram (°C).

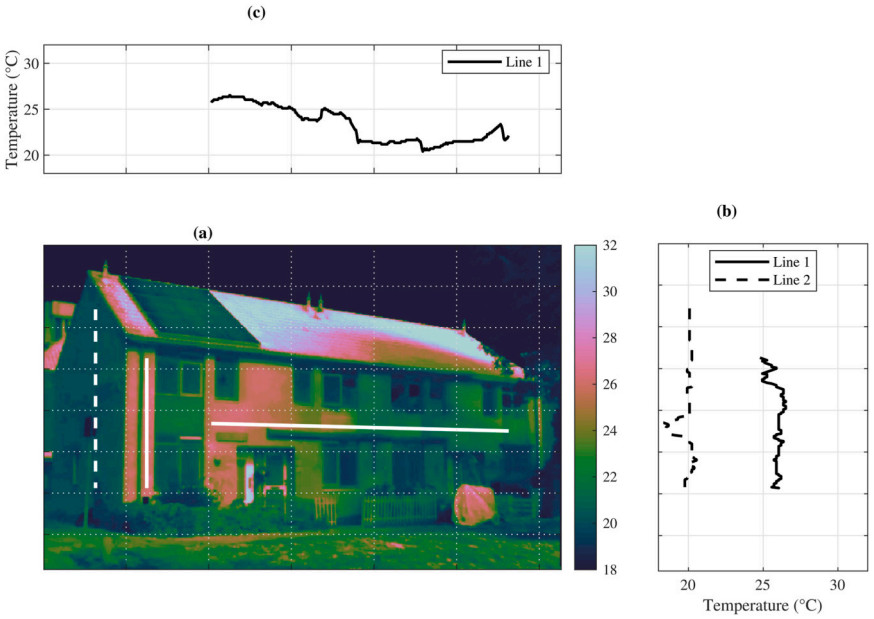

FIGURE 10
Horizontal and vertical temperature profiles along the surface of the façades of an existing masonry building in Scheepmakerij, Delft. **(a)** Processed thermal image. **(b)** Vertical temperature profiles. **(c)** Horizontal temperature profiles.

practice that temperature fluctuations can induce cracking damage, hence the use of expansion and movement joints in the design of new buildings, the severity and extent of such damage have not been systematically quantified. Moreover, the magnitude of daily and/or seasonal temperature differences on the surface of external walls has not been assessed.

As discussed in the previous sections, specific insights can be drawn from a limited number of studies employing thermographic analysis to assess temperature gradients over wall surfaces. Although these studies did not aim to characterize the resulting structural damage, they observed that different portions of a wall can experience temperature differentials ranging from 7 °C to 17 °C, depending on sun orientation, time of day, and shading conditions (Na et al., 2016; Vollmer and Möllmann, 2018; Barbero-Barrera et al., 2024). Nevertheless, these studies do not provide sufficient information to characterize the spatial distribution of temperature variations over wall surfaces. In this study, ΔT values of up to about 10 °C are observed from the outing, which are well within the ranges reported in the aforementioned studies; precise values are indeed dependent on specific environmental conditions and the surface

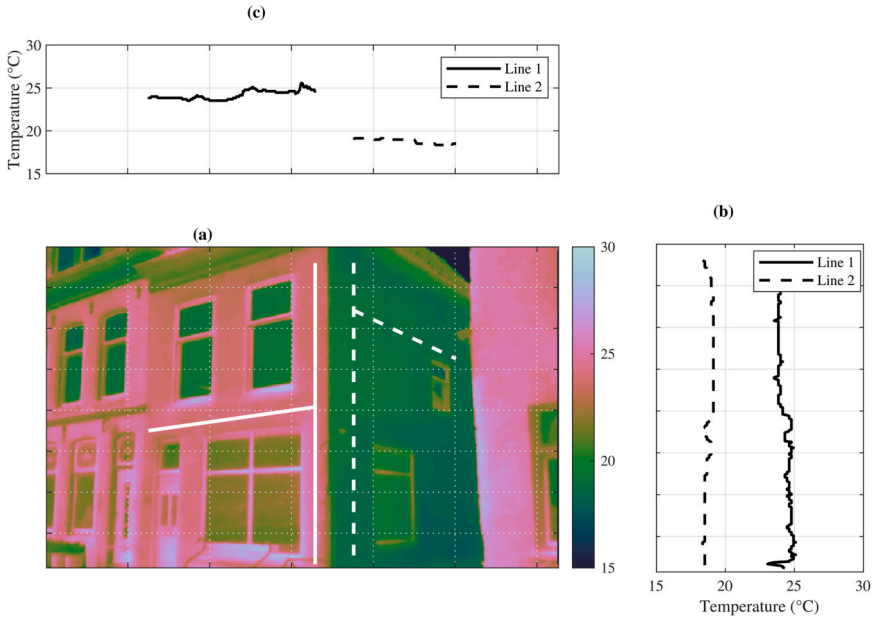

FIGURE 11
Horizontal and vertical temperature profiles along the surface of the façades of an existing masonry building in Delft city center. **(a)** Processed thermal image. **(b)** Vertical temperature profiles. **(c)** Horizontal temperature profiles.

finish and color of the masonry. Moreover, temperature differences of 5 °C–6 °C are observed between perpendicular façades when one is in the shadow and another under direct solar irradiation. In this light, the values observed are consistent with literature yet provide further information regarding the spatial variability of surface temperatures of external masonry walls.

4.2 Limitations and recommendations

In this study, outdoor thermography is used to acquire measurements of temperature values over external wall surfaces. The differences between the maximum and minimum temperature, and their spatial distribution, are discussed, providing insight into the potential ΔT on external masonry wall surfaces of existing old buildings.

The accuracy and reliability of the results depend on the quality of the measurements, which should ideally be carried out by a skilled and experienced operator to ensure dependable outcomes (Hart, 1991; Richter and Fouad, 2021). Furthermore, as noted in the previous sections, the IR camera automatically compensates for emissivity, object distance, ambient temperature, relative humidity, and apparent object temperature, provided these values are given as inputs. In this study, all image acquisitions were performed using consistent parameters (reported in Table 1), chosen based on the weather conditions during the field excursions. The underlying assumption is that such parameters may have a significantly greater impact on the absolute temperature values, but less on their differences and spatial distribution, which are the key objectives of this study.

To test this hypothesis, a comparison is carried out with two images of the same building with different camera parameters (Figure 12). The infrared camera employed allows for a posteriori reprocessing of the original images by adjusting the input parameters. Specifically, the results previously presented in Figure 7 (and reproduced in Figures 12a1–c1) were reprocessed using arbitrarily selected extreme values of the input parameters to evaluate their influence (Figures 12a2–c2). The histogram in Figure 12c2 shows that, with the modified parameters, the temperature distribution shifts to lower values and slightly broadens, with a peak around 27 °C–29 °C, compared to the previous peak of 31 °C–33 °C. Nevertheless, the distributions represented in both histograms exhibit a consistent shape.

Overall, the ΔT values in the two images appear consistent. In Figure 12c1, ΔT is 13 °C, ranging from 21 °C to 34 °C, while in Figure 12c2, ΔT is 15 °C, ranging from 16 °C to 31 °C. The spatial distribution is also in good agreement, with lower temperatures observed at the bottom left of the wall and higher temperatures at the top right. When discussing the differences, it should be noted that the values in Figures 12a2–c2 represent extreme cases resulting from very extreme input parameters, used specifically for the sensitivity analysis. Overall, the parameters listed in Table 1 are considered a reasonable choice for the field excursions. Hence, were these parameters slightly different than assumed during the thermographic excursions, their influence on the temperature differentials registered on the brick masonry façades would be negligible. This includes minor differences in brick material and weathered (aged) condition.

The thermographic images and results presented here a limited to a single excursion conducted in early September of 2025. While earlier excursions were performed to develop the methods presented herein, the consistent study was carried out on a single day. This excusion was sufficient to establish that temperature gradients appear on masonry walls due to solar irradiation; moreover, possible magnitude of these differentials were also registered.

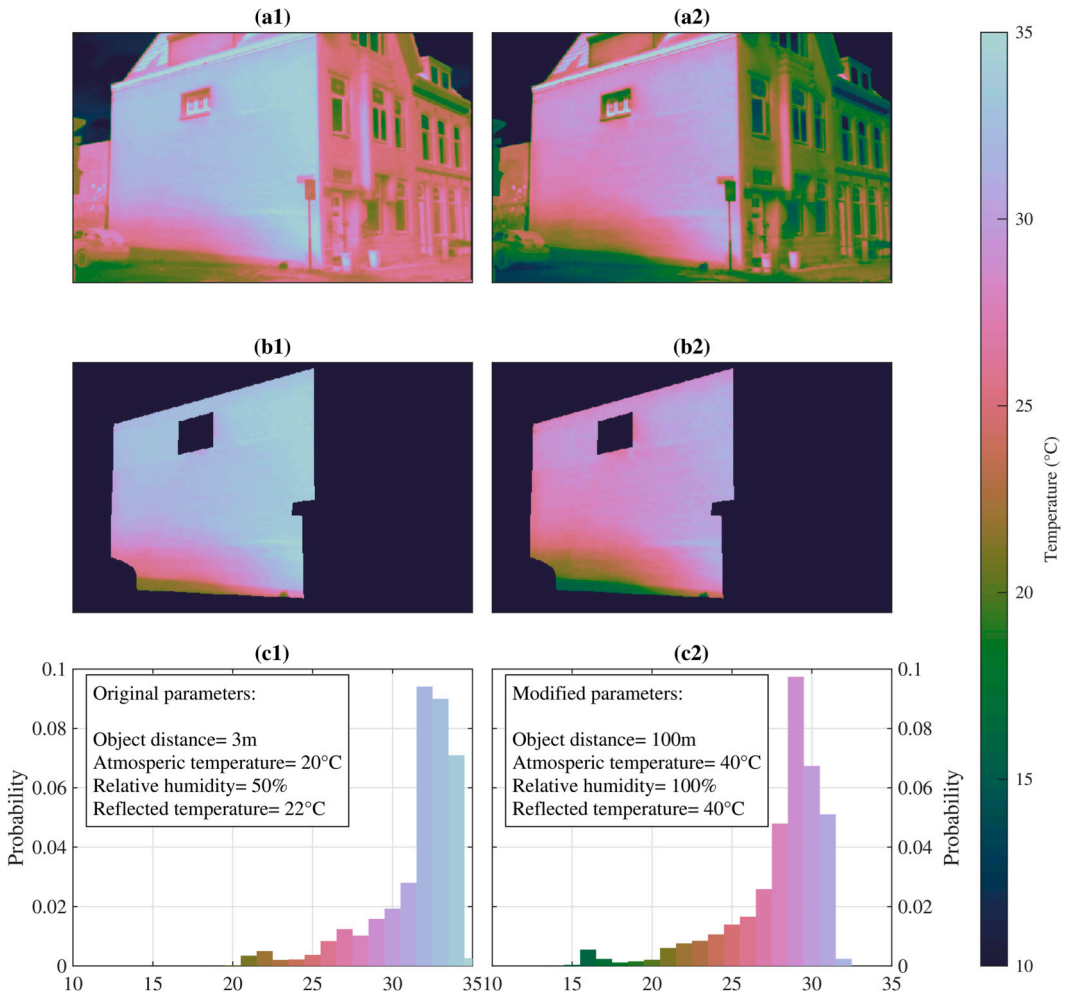

FIGURE 12
Comparison between thermal image captured using the IR camera settings listed in Table 1 ((**a1–c1**), as previously shown in Figure 7), and the same image with the modified parameters **(a2–c2)**.

With a single excursion, is not possible to conclude whether these measurements are representative of typical conditions. Yet, such an observation is not necessary to claim that temperature gradients are a potential hazard to brick structures. Indeed, the findings demonstrate the existence and plausible magnitude of spatial ΔT under real outdoor conditions, rather than providing a climatological characterization of frequency or seasonal extremes.

Based on the findings of this study, several recommendations for future research are proposed:

1. More extensive thermographic analyses should be conducted across diverse building types, orientations, and environmental conditions to enhance understanding of spatial temperature gradients.
2. Methods should be developed to accurately map the spatial distribution of temperature variations on wall surfaces, employing high-resolution imaging and advanced data processing techniques.
3. Controlled experiments on masonry wall specimens are recommended to directly measure temperature gradients and validate observational findings.
4. Further research examining the impact of such temperature gradients on cracking and other forms of masonry damage is required to establish clear relationships between thermal variations and structural damage, either employing tests in controlled conditions or computational simulations, as for instance the preliminary analyses in Longo et al. (2025).
5. Based on environmental conditions and shading, methods should be developed to predict temperature gradients across exterior walls, with the aim of linking these gradients to potential damage or material degradation.

4.3 Potential implications of this research

The results of this study indicate that the exterior walls of older masonry buildings are exposed to temperature variations across their surfaces. This observation has several important implications. From a hygrothermal perspective, certain areas of the walls may experience sharp temperature increases or decreases. This process can have an impact on the heat loss and energy consumption of the building. Mechanically, such variations can induce localized stresses,

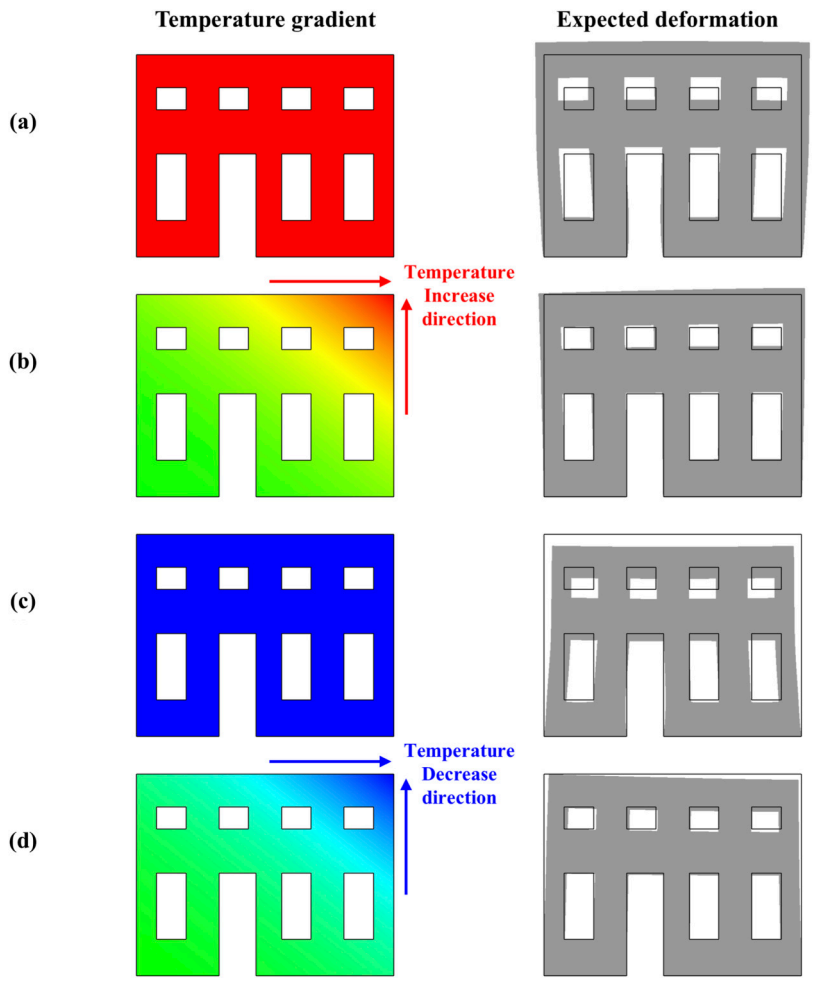

FIGURE 13
Schematic examples illustrating the expansion and contraction of a masonry façade with restrained movement at its base but unrestrained at the top and sides, in response to uniform temperature changes, either an increase **(a)** or a decrease **(c)**, and bidirectional temperature changes, either an increase **(b)** or a decrease **(d)**.

potentially contributing to wall deterioration and cracking damage. The formation of cracks, even minor ones, can compromise the wall's water tightness or impermeability (Gaggero et al., 2024), allowing increased rainwater penetration, which might lead to further damage. Furthermore, even small, purely aesthetic cracks can negatively affect the occupants' sense of safety (Rots, 1994).

Figure 13 schematically illustrates how a masonry wall, restrained at its base by the foundation but unrestrained at the top and sides, would deform under different temperature variations. Although the figure is a simplified sketch, it shows that under a symmetric temperature change, the wall experiences expansion in the mid-to-upper region during uniform heating, and contraction during uniform cooling (Figures 13a,c). These regions are likely to be the initial locations of damage in an almost symmetric veneer, particularly around weaker areas such as window corners (Farmer and Gerns, 2010; Holland, 2023). When the temperature distribution is non-uniform, the locations of potential damage shift (Figures 13b,d). These patterns may influence where damage first appears, which could affect diagnostic surveys and maintenance strategies.

Even when no temperature differences were observed across the surface of a single wall, variations were still detected between the wall and its connected perpendicular walls (Figures 10, 11). This could trigger both in-plane and out-of-plane deformations of the building's exterior.

Preliminary numerical models with thermo-mechanical coupling suggest that at a temperature differential of 10 °C (between the coolest and warmest point in a façade), visible cracks of 0.1 mm in width may appear. Moreover, when a stark contrast in temperature arises between orthogonal façades, vertical cracks are expected near the corners when these walls are well connected (see Figure 1c); numerical models estimate that visible cracks appear with only 5 °C difference between the walls. These complex calculations, however, are beyond this study and require substantial, additional investigation; they are provided here only as a frame of reference.

Depending on the orientation and location of the buildings, some exterior walls may be more exposed to environmental actions combined with temperature-related cracking. Such cracking can contribute to the gradual deterioration of the wall's structural

performance, making it more vulnerable to additional sources of damage over time (Gonçalves et al., 2015).

Overall, the empirical insights provided by this study are expected to serve as a basis for further analyses investigating the impact of such temperature variations.

5 Conclusion

This study investigated the spatial distribution of temperature variations (ΔT) over the surfaces of exterior masonry walls using outdoor IR thermography and post-processing techniques. The findings contribute to a better understanding of the magnitude of temperature differences and their spatial distribution, which may lead to structural damage in existing old buildings.

Based on the results of the analysis, it has been observed that:

- Temperature values over external façades are not always uniform and may present variations vertically (in the direction of the wall height) and/or horizontally (along the wall length).
- Maximum temperature differences (ΔT) between different points on the surface of typical masonry walls of residential buildings were measured up to 10 °C–13 °C.
- Temperature differences of 5 °C–6 °C are observed between the front (street) façade and perpendicular transversal walls; vertical profiles confirmed similar inter-wall differences.
- The distributions of the temperature values measured over exterior walls resemble lognormal distributions, indicating that extreme values are localized.
- Existing literature lacks a systematic quantification of thermal-induced structural damage; this study contributes by mapping spatial temperature variations.
- The methodology employed is proposed for the assessment of temperature differences over external wall surfaces and their spatial patterns, supporting its use in structural diagnostics.

Data availability statement

The raw data supporting the conclusions of this article will be made available by the authors, without undue reservation.

Author contributions

AP: Methodology, Investigation, Conceptualization, Software, Writing – review and editing, Writing – original draft, Formal Analysis, Validation, Visualization, Data curation. PK: Funding acquisition, Supervision, Writing – review and editing, Project administration, Conceptualization. ML: Conceptualization, Writing – review and editing. JR: Funding acquisition, Conceptualization, Writing – review and editing.

Funding

The author(s) declared that financial support was not received for this work and/or its publication.

Acknowledgements

The authors would like to acknowledge the contribution of Instituut Mijnbouwschade Groningen (IMG) and Commissie Mijnbouwschade (CM) for inspiring this study.

Conflict of interest

The author(s) declared that this work was conducted in the absence of any commercial or financial relationships that could be construed as a potential conflict of interest.

Generative AI statement

The author(s) declared that generative AI was used in the creation of this manuscript. The isometric view of the building presented in Figure 6 was generated using Google's Gemini 2.5 Flash Image generative AI model, which is hosted on the Gemini platform. Besides facilitating the illustration with the AI tool, the Authors curated the data, analyses, and the manuscript.

Any alternative text (alt text) provided alongside figures in this article has been generated by Frontiers with the support of artificial intelligence and reasonable efforts have been made to ensure accuracy, including review by the authors wherever possible. If you identify any issues, please contact us.

Publisher's note

References

Almherigh, M. A. (2014). Common causes of cracking in masonry walls diagnosis and remedy. *Int. J. Sci. Basic Appl. Res.* 14 (1), 25–33.

Arslan, O., Messali, F., Smyrou, E., Bal, I. E., and Rots, J. G. (2021). Experimental characterization of the axial behavior of traditional masonry wall metal tie connections in cavity walls. *Constr. Build. Mater.* 266, 121141. doi:10.1016/j.conbuildmat.2020.121141

Athauda, R. S., Asmone, A. S., and Conejos, S. (2023). Climate change impacts on facade building materials: a qualitative study. *Sustainability* 15 (10), 7893. doi:10.3390/su15107893

Balaras, C. A., and Argiriou, A. (2002). Infrared thermography for building diagnostics. *Energy Buildings* 34 (2), 171–183. doi:10.1016/s0378-7788(01)00105-0

Barbero-Barrera, M. D. M., Tendero-Caballero, R., and García de Viedma-Santoro, M. (2024). Impact of solar shading on façades' surface temperatures under summer and winter conditions by IR thermography. *Architecture* 4 (2), 221–246. doi:10.3390/architecture4020014

Barreira, E., and de Freitas, V. P. (2007). Evaluation of building materials using infrared thermography. *Constr. Building Materials* 21 (1), 218–224. doi:10.1016/j.conbuildmat.2005.06.049

Bauer, E., Milhomem, P. M., and Aidar, L. A. G. (2018). Evaluating the damage degree of cracking in facades using infrared thermography. *J. Civ. Struct. Health Monit.* 8 (3), 517–528. doi:10.1007/s13349-018-0289-0

Beran, P. (2012). The influence of solar radiation on the distribution of temperatures in historic masonry. *WIT Trans. Eng. Sci.* 75, 181–192.

BRE (1995). Assessment of damage in low-rise buildings, with particular reference to progressive foundation movement. *BRE Garst. Watford*.

Brick Industry Association (2006). Volume changes—Analysis and effects of movement. *Tech. Notes Brick Constr.*, 1–3.

Brimblecombe, P., and Grossi, C. M. (2007). Damage to buildings from future climate and pollution. *APT Bull. J. Preserv. Technol.* 38 (2/3), 13–18.

Chauhan, D., Khan, T., Tripathi, D., Mishra, D., and Singh, A. (2020). *Causes, prevention and repair of cracks*. Babu Banarasi Das University.

Chew, M. (1998). Assessing building façades using infra-red thermography. *Struct. Surv.* 16 (2), 81–86. doi:10.1108/02630809810219669

Chitte, C. J., and Sonawane, Y. N. (2018). Study on causes and prevention of cracks in building. *Int. J. Res. Appl. Sci. Eng. Technol.* 6 (3), 453–461. doi:10.22214/ijraset.2018.3073

Chouidira, M., Ihaddadene, N., Zggane, H., and Ihaddadene, R. (2022). "Effect of solar radiation on the temperature of house walls facing the four cardinal points in the summer in ouled Sidi brahim (algeria)," in *2022 13th international renewable energy congress (IREC)* (IEEE), 1–6.

De Vent, I. A. E. (2011). Structural damage in masonry: developing diagnostic decision support.

Dilrukshi, K., and Dias, W. (2008). Field survey and numerical modelling of cracking in masonry walls due to thermal movements of an overlying slab.

Dilrukshi, K., and Dias, W. (2010). Physical modelling for investigation of cracking in masonry walls due to thermal movements of an overlying slab.

Duan, Z., de Wilde, P., Attia, S., and Zuo, J. (2025). Challenges in predicting the impact of climate change on thermal building performance through simulation: a systematic review. *Appl. Energy* 382, 125331. doi:10.1016/j.apenergy.2025.125331

Elizalde, R. R. (2025). Thermography applied to old masonry constructions.

Farmer, M., and Gerns, E. (2010). "Design and use of expansion joints in new and existing clay masonry wall systems," in *Symposium on masonry* (ASTM International), 170–195.

Flir Systems, I. (2017). User's manual FLIR exx series.

Flir Systems, I. (2019). *Thermography reference documentation: T810442*. FLIR Systems, Inc.

Flir Systems, I. (2024). FLIR Exx-SERIES advanced thermal imaging cameras - FLIR exx matrix (LTR incl E52) en-US.pdf.

Gaggero, M. B., Korswagen, P. A., Esposito, R., and Rots, J. G. (2024). Innovative application of self-healing technology to masonry: a proof of concept. *Int. J. Archit. Herit.* 19, 1–11. doi:10.1080/15583058.2024.2380408

Gohnert, M. (2012). The effects of thermal loading on masonry structures. *Key Engineering Materials* 517, 689–694. doi:10.4028/www.scientific.net/kem.517.689

Gonçalves, A., De Brito, J., and Amaro, B. (2015). Systematic approach to inspect, diagnose, and repair masonry walls. *J. Perform. Constr. Facil.* 29 (6), 04014155. doi:10.1061/(asce)cf.1943-5509.0000650

Grandić, D., Šćulac, P., Ružić, I., and Krvavica, N. (2019). "Crack monitoring in the baptistery of the euphrasian basilica in poreč," in *5th international conference on smart monitoring, assessment and rehabilitation of civil structures* (Empa–Swiss Federal Laboratories for Materials Science and Technology).

Hart, J. (1991). A practical guide to infra-red thermography for building surveys.

Holland, M. (2023). *Practical guide to diagnosing structural movement in buildings*. John Wiley and Sons.

Huijbregts, Z., Kramer, R., Martens, M., Van Schijndel, A., and Schellen, H. (2012). A proposed method to assess the damage risk of future climate change to museum objects in historic buildings. *Build. Environ.* 55, 43–56. doi:10.1016/j.buildenv.2012.01.008

Kadaster (2018). Praktijkhandleiding bag - handleiding bij de catalogus van de basisregistratie adressen en gebouwen.

Kapusta, Ł., and Szojda, L. (2021). The role of expansion joints for traditional buildings affected by the curvature of the mining area. *Eng. Fail. Anal.* 128, 105598. doi:10.1016/j.engfailanal.2021.105598

Kim, H., Lamichhane, N., Kim, C., and Shrestha, R. (2023). Innovations in building diagnostics and condition monitoring: a comprehensive review of infrared thermography applications. *Buildings* 13 (11), 2829. doi:10.3390/buildings13112829

Kleinfeld, J. (2004). Infrared for detection of exterior wall moisture and delamination: a case study and comparison to FEA predictions. *InfraMation 2004 Proc.* 5, 45–57.

Lacasse, M. A., Gaur, A., and Moore, T. V. (2020). Durability and climate change—Implications for service life prediction and the maintainability of buildings. *Buildings* 10 (3), 53. doi:10.3390/buildings10030053

Latifi, R., Hadzima-Nyarko, M., Radu, D., and Rouhi, R. (2023). A brief overview on crack patterns, repair and strengthening of historical masonry structures. *Materials* 16 (5), 1882. doi:10.3390/ma16051882

Longo, M., Korswagen Eguren, P., and Rots, J. (2025). "Numerical simulations of temperature variations in historical masonry façades considering soil," in *14th international conference on structural analysis of historical constructions (SAHC 2025)* (Lausanne, Switzerland).

Maksoud, A., Al-Beer, H. B., Hussien, A. A., Dirar, S., Mushtaha, E., and Yahia, M. W. (2023). Computational design for futuristic environmentally adaptive building forms and structures. *Archit. Eng.* 8 (1), 13–24. doi:10.23968/2500-0055-2023-8-1-13-24

Marino, B. M., Muñoz, N., and Thomas, L. P. (2017). Estimation of the surface thermal resistances and heat loss by conduction using thermography. *Appl. Therm. Eng.* 114, 1213–1221. doi:10.1016/j.applthermaleng.2016.12.033

Masciotta, M.-G., Ramos, L. F., Lourenço, P. B., and Matos, J. A. (2016). "Development of key performance indicators for the structural assessment of heritage buildings," in *8th European workshop on structural health monitoring, EWSHM*, 606.

Messali, F., Esposito, R., Jafari, S., Ravenshorst, G., Korswagen, P., and Rots, J. G. (2018). "A multiscale experimental characterisation of Dutch unreinforced masonry buildings," in *16th European conference on earthquake engineering, thessaloniki*.

Miranda Dias, J., Matias, L., and Henriques, M. J. (2021). Masonry walls of buildings with reinforced concrete structure-detection of cracking due to the effect of temperature variations through NDT techniques.

Mrozek, D., Mrozek, M., and Fedorowicz, J. (2017). Analysis of an effectiveness of expansion joints in the multi-family building loaded by mining activities. *Czas. Inżynierii Lądowej, Środowiska I Archit.* 64 (2/II), 199–210.

Na, R., Shang, Z., and Shen, Z. (2016). "Time-lapse of cavity brick wall temperature profiles using infrared thermography," in *Proceedings of the 52nd ASC annual international conference* (Provo, UT, USA).

Niedostatkiewicz, M., and Majewski, T. (2024). Causes of defects and damage to brick masonry elements in historic buildings. *Civ. Environ. Eng. Rep.* 34, 423–448. doi:10.59440/ceer/194876

Ottoni, F., and Blasi, C. (2015). Results of a 60-year monitoring system for Santa Maria del Fiore Dome in Florence. *Int. J. Archit. Herit.* 9 (1), 7–24. doi:10.1080/15583058.2013.815291

O'Connor, T. F., and Droz, H. L. (1996). "Design considerations for sealants when used at horizontal expansion joints in masonry cavity walls," in *Science and technology of building seals, sealants, glazing, and waterproofing*. Sixth Volume (ASTM International), 63–83.

Pellegrini, D., Barontini, A., Mendes, N., and Lourenço, P. B. (2024). Dynamic response of masonry structures to temperature variations: experimental investigation of a brick masonry wall. *Sensors* 24 (23), 7573. doi:10.3390/s24237573

Peters, R., Dukai, B., Vitalis, S., van Liempt, J., and Stoter, J. (2022). Automated 3D reconstruction of LoD2 and LoD1 models for all 10 million buildings of the Netherlands. *Photogramm. Eng. Remote Sensing* 88 (3), 165–170. doi:10.14358/PERS.21-00032R2

Playà-Montmany, N., and Tattersall, G. J. (2021). Spot size, distance and emissivity errors in field applications of infrared thermography. *Methods Ecol. Evol.* 12 (5), 828–840. doi:10.1111/2041-210x.13563

Plesu, R., Teodoriu, G., and Taranu, G. (2012). Infrared thermography applications for building investigation. *Bul. Institutului Politehnic Din. Lasi. Sect. Constr. Arhit.* 58 (1), 157.

Prosperi, A. (2025). *Modelling of subsidence induced damage to masonry buildings: influence of soil heterogeneity on settlement and development of fragility curves*. Delft University of Technology.

Prosperi, A., Korswagen, P. A., Longo, M., Korff, M., and Rots, J. G. (2025a). Toward NLFEA-based fragility curves for unreinforced masonry buildings exposed to subsidence. *J. Build. Eng.* 112, 113676. doi:10.1016/j.jobe.2025.113676

Prosperi, A., Longo, M., Korswagen, P. A., Giardina, G., and Rots, J. G. (2025b). Comparative study of NLFE models for simulating settlement-induced damage in masonry façades: macro-and simplified micro-models. *Front. Built Environ.* 11, 1618329. doi:10.3389/fbuil.2025.1618329

Prosperi, A., Longo, M., Korswagen, P. A., Korff, M., and Rots, J. G. (2025c). "Damage from ups and downs: investigating cracking in unreinforced masonry structures exposed to settlement and uplift cycles using finite element analyses," in *15th Canadian masonry symposium*.

Ramirez, R., Ghiassi, B., Pineda, P., and Lourenço, P. B. (2023). Hygro-thermo-mechanical analysis of brick masonry walls subjected to environmental actions. *Appl. Sci.* 13 (7), 4514. doi:10.3390/app13074514

Ramirez, R., Ghiassi, B., Pineda, P., and Lourenço, P. B. (2024). "Moisture and temperature effects on masonry structures: the civic tower of Pavia as a case study," in *International brick and block masonry conference* (Springer), 845–865.

Richter, T., and Fouad, N. A. (2021). *Guidelines for thermography in architecture and civil engineering: theory, application areas, practical implementation*. Birkhäuser.

Roberts, S. (2008). Effects of climate change on the built environment. *Energy Policy* 36 (12), 4552–4557. doi:10.1016/j.enpol.2008.09.012

Rots, J. (1994). Structural masonry: an experimental/numerical basis for practical design rules.

Sansara, P. (2023). Effect of temperature on performance of crack repair materials on rendered walls.

Selvarajah, S., and Johnston, A. (1995). Water permeation through cracked single skin masonry. *Build. Environ.* 30 (1), 19–28. doi:10.1016/0360-1323(94)e0033-n

Smith, A. S., and Edgell, G. J. (2009). "Chapter 35: defects in masonry walls," in *ICE manual of construction materials: volume I: fundamentals and theory; concrete; asphalts in road construction; masonry*. Editor M. Forde (Emerald Publishing Limited).

Thagunna, G. (2014). "Building cracks–causes and remedies," in *3rd world conference on applied sciences* (Engineering and Technology at Basha Research Centre).

Usamentiaga, R., Venegas, P., Guerediaga, J., Vega, L., Molleda, J., and Bulnes, F. G. (2014). Infrared thermography for temperature measurement and non-destructive testing. *Sensors* 14 (7), 12305–12348. doi:10.3390/s140712305

van Aarle, M., Schellen, H., and van Schijndel, J. (2015). Hygro thermal simulation to predict the risk of frost damage in masonry; effects of climate change. *Energy Procedia* 78, 2536–2541. doi:10.1016/j.egypro.2015.11.268

Van Zijl, G., and Verhoef, L. (2001). "Computational assessment of renovation intervention in a historic masonry building," in *Proc., 9th Canadian masonry symp*. Editors P. H. Bischoff, J. L. Dawe, A. B. Schriver, and A. J. Valsangkar (New Brunswick, Canada: CD ROM).

Van Zijl, G., De Vries, P., and Vermeltfoort, A. (2004). Masonry wall damage by restraint to shrinkage. *J. Struct. Eng.* 130 (7), 1075–1086. doi:10.1061/(asce)0733-9445(2004)130:7(1075)

Vollmer, M., and Möllmann, K.-P. (2018). *Infrared thermal imaging: fundamentals, research and applications*. John Wiley and Sons.

Xia, Q., Liu, X., Li, Y., Xiong, Y., and Wu, Q. (2025). Multiscale study on the damage of ancient masonry structures under the coupled action of heat and moisture. *Constr. Build. Mater.* 490, 142453. doi:10.1016/j.conbuildmat.2025.142453

Yan, L., Tonghui, W., and Hui, N. (2015). "The simple simulation study of temperature cracks in masonry structure wall," in *2015 sixth international conference on intelligent systems design and engineering applications (ISDEA)* (IEEE), 894–897.

Yang, X., Li, Y., and Yang, L. (2012). Predicting and understanding temporal 3D exterior surface temperature distribution in an ideal courtyard. *Build. Environ.* 57, 38–48. doi:10.1016/j.buildenv.2012.03.022

Yemer, F. M. (2010). *Urban wind map for delft, rotterdam and zoetermeer*. Masters Thesis Delft University of Technology.